Author's version
Published in
Environmental Science & Technology 46(7), pp 4008-4015
DOI: 10.1021/es202643c
http://dx.doi.org/10.1021/es202643c

Transport of ferrihydrite nanoparticles in saturated porous media: role of ionic strength and flow rate

Tiziana Tosco[(1)], Julian Bosch[(2)], Rainer U. Meckenstock[(2)], and Rajandrea Sethi[(1)] (*)

(1) Dipartimento di Ingegneria dell'Ambiente, del Territorio e delle Infrastrutture, Politecnico di Torino, corso Duca degli Abruzzi 24, 10129 Torino, Italy

(2) Helmholtz Zentrum München - German Research Center for Environmental Health, Institute of Groundwater Ecology, Ingolstädter Landstr. 1, D-85764 Neuherberg, Germany

E-mail addresses: tiziana.tosco@polito.it, julian.bosch@helmholtz-muenchen.de, rainer.meckenstock@gsf.de, rajandrea.sethi@polito.it

14th February, 2012

Title running head: Transport of ferrihydrite nanoparticles in saturated porous media

(*) Corresponding author: Dr. Rajandrea Sethi, Dipartimento di Ingegneria dell'Ambiente, del Territorio e delle Infrastrutture, Politecnico di Torino, corso Duca degli Abruzzi 24, 10129 Torino, Italy. E-mail: rajandrea.sethi@polito.it. Phone: +390115647735. Fax: +390115647699

ABSTRACT: The use of nanoscale ferrihydrite particles, which are known to effectively enhance microbial degradation of a wide range of contaminants, represents a promising technology for in situ remediation of contaminated aquifers. Thanks to their small size, ferrihydrite nanoparticles can

be dispersed in water and directly injected into the subsurface to create reactive zones where contaminant biodegradation is promoted. Field applications would require a detailed knowledge of ferrihydrite transport mechanisms in the subsurface, but such studies are lacking in the literature. The present study is intended to fill this gap, focusing in particular on the influence of flow rate and ionic strength on particle mobility. Column tests were performed under constant or transient ionic strength, including injection of ferrihydrite colloidal dispersions, followed by flushing with particle-free electrolyte solutions. Particle mobility was greatly affected by the salt concentration, and particle retention was almost irreversible under typical salt content in groundwater. Experimental results indicate that, for usual ionic strength in European aquifers (2 to 5 mM), under natural flow condition ferrihydrite nanoparticles are likely to be transported for 5 to 30 m. For higher ionic strength, corresponding to contaminated aquifers, (e.g. 10 mM) the travel distance decreases to few meters. A simple relationship is proposed for the estimation of travel distance with changing flow rate and ionic strength. For future applications to aquifer remediation, ionic strength and injection rate can be used as tuning parameters to control ferrihydrite mobility in the subsurface and therefore the radius of influence during field injections.

KEYWORDS: ferrihydrite, environmental nanominerals, anaerobic contaminant degradation, groundwater remediation, colloid transport

TOC ART

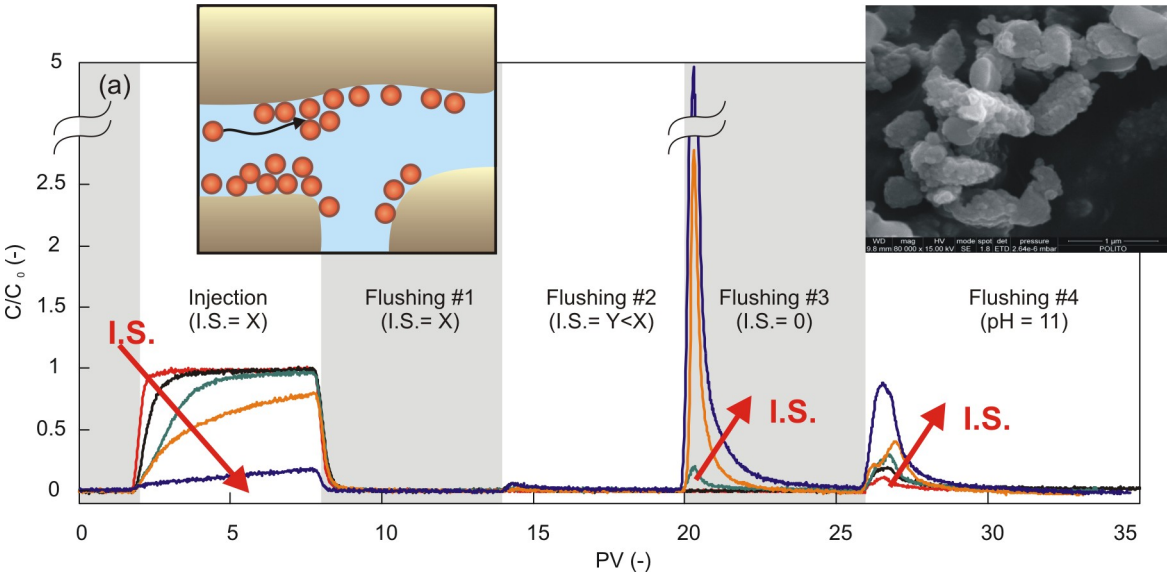

Introduction

Nanoparticles are gaining increased attention in environmental applications thanks to their high reactivity, opening a new perspective on the rates of mass and electron turnover in biogeochemical systems *(1-3)*. This has also been true for microbial iron reduction *(4-6)*, which is a major pathway for anaerobic respiration *(7)*. Previous studies showed that iron oxide nanoparticles *(8)*, and in particular nanosized ferrihydrite *(4, 9)*, exhibit an extreme reactivity and bioavailability, higher by up to an order of magnitude than macroaggregate oxides *(10)*. This was also attributed to the superior stability of these negatively charged colloids at groundwater pH and ionic strength. In subsurface environments, microbial iron reduction is frequently linked to contaminant oxidation, as many iron-reducing bacteria are capable of metabolizing a wide range of organic substrates, including recalcitrant water contaminants *(11-14)*. Consequently, the high reactivity of nanosized iron oxides as electron acceptors in microbial iron reduction opens perspective of application in the field of groundwater remediation.

Unlike other colloids used for groundwater remediation (eg. nano- and microscale zerovalent iron) *(15-16)*, ferrihydrite particles dispersed in water form a stable dispersion, without requiring addition of polymers to improve stability against aggregation and/or sedimentation. They can be stored in deionized water at relatively high concentrations without showing significant sedimentation, nor undergoing relevant modifications of their chemical properties *(4)*. This greatly facilitates their handling for field applications. Nevertheless, nanoparticles are known to be sensitive to fluctuations of ionic strength and other hydrochemical parameters *(17)*, which determine the stability of their colloidal suspension.

Even if the reactivity of ferrihydrite nanoparticles is quite well known at the moment, the use of such nanoparticles as an electron acceptor for in situ biodegradation would require a deep knowledge of their mobility in porous media. Despite several studies were focused on the transport

of natural and synthetic colloids, to the authors' knowledge no investigation has been performed on ferrihydrite nanoparticles. The mobility of ferrihydrite particles in porous media is expected to be ruled by transport mechanisms similar to those controlling well-studied natural *(18-20)* and synthetic colloids *(21-22)*. At the pore scale, colloid mobility is controlled by physico-chemical interactions among particles and porous medium, which result in dynamic deposition and release phenomena *(23-24)*. A major role in deposition and release processes is played by the surface charge of both colloids and porous medium, the chemical composition of pore water *(22, 25-26)* and the flow rate *(27-28)*.

This work aims at understanding how the abovementioned mechanisms control the transport of ferrihydrite colloids in porous media, and how hydrological and hydrochemical parameters (in particular, ionic strength and flow rate) can be used to control the mobility of the particles in the subsurface. Column transport tests were performed injecting ferrihydrite nanoparticles through saturated sand-packed columns at concentrations used in field applications. The influence of dissolved ions, in the typical range of groundwater ionic strength *(29)*, was investigated under different flow rates in both stationary and transient hydrochemical conditions. Finally, a correlation is proposed and applied to estimate the travel distance that can be expected in field injections.

Materials and Methods

Colloid dispersions synthesis

Colloidal particles of ferrihydrite were synthesised following the protocol described in *(30)*. 20.95 g of ferric citrate powder (cell culture tested, Sigma) were suspended in ~ 300 ml MilliQ-H_2O, using vigorous stirring and heating to 80°C (~1h). Once the solution contained no more ferric citrate particles, it was cooled down to room temperature. Then the pH was quickly adjusted to 8.0 using 10 M NaOH while stirring. After this the solution was left stirring heavily for 30 min and filled to a final volume of 500 ml. Then the solution was centrifuged at 8000 G for 1h at 4°C. The

supernatant was discarded and the pellet resuspended in MilliQ-H_2O by shaking. The centrifugation-resuspension cycles were repeated 4 times to remove residual ions and citrate from synthesis. A mean hydrodynamic radius of 106.7±15.5 nm was measured with dynamic light scattering (DLS, Zetasizer Nano ZS90, Malvern Instruments Ltd, UK). The colloidal dispersion in MilliQ water was stable over a period of months.

The same DLS equipment was also used to measure the electrokinetic properties of the colloidal particles. Nanoparticles were dispersed in the background solutions used in column tests, that is, DI water, water with addition of NaCl (1 mM, 3 mM, 5 mM and 10 mM), and water with pH 10 via addition of NaOH 1 mM. Sonication was applied immediately after particle dilution, to avoid the formation of aggregates. Measurements were performed 2 hours after sample preparation, without further shaking. Electrokinetic mobility of the ferrihydrite colloids was analyzed by DLS in non-invasive backscattering detection (Nano ZS, Malvern Instruments, Malvern, UK). Two measurements were conducted per sample with 10 runs per measurement at a collection time of 10 s per run. All data met the quality criteria with an autocorrelation function > 0.94.

Columns

Quartz sand (nominal SiO_2 content 98.9%) with a minor content of K-feldspar and a mean diameter d_{50} of 0.194 mm (Dorsilit 8, Dorfner) was used for wet packing of a chromatographic column with an inner diameter of 16 mm. Mobile adaptors were used at column ends. A fixed amount of 34.7 g of dry sand was used for each column, corresponding to an average column length of 11.2(±0.1) cm. Porous medium parameters were determined via inverse fitting of breakthrough curves of NaCl as a conservative tracer, resulting in an average effective porosity of 0.447(±0.021) and an average dispersivity of $2.82(\pm0.62)\cdot10^{-4}$ m.

The absence of organic matter absorbed on sand grains was ensured by cindering. Prior to use, the sand was thoroughly cleaned by means of a number of sonication cycles in, respectively, tap water,

DI water and NaOH concentrated solution, in order to remove all residual colloids. Finally, it was thoroughly rinsed with DI water and then degassed to allow a complete hydration of the grains. Blank column tests, run as controls injecting particle-free solutions at the same ionic strengths used for transport tests, did not show any relevant release of colloids.

The concentration of salt and colloidal particles at column inlet and outlet was monitored on line via optical density measurements, using a UV-vis spectrophotometer (Specord S600, Analytik Jena, Germany) equipped with flow-through cells characterized by a 10 mm light path, 80 µl chamber volume (Hellma, Germany). Basing on calibration curves, monitoring wavelengths of 198.5 nm for NaCl and NaOH, 400 nm for the colloids were chosen, which showed a linear relationship between absorbance and concentration.

Experimental protocol for transport experiments

Ferrihydrite colloids were dispersed in water (eventually with addition of NaCl) at a particle concentration of 7.5 mg/l. The ionic strength ranged from MilliQ water (electrical conductivity ~ 20 µS cm^{-1}) to 10 mM NaCl (~ 1900 µS cm^{-1}), which corresponds to the typical ionic strength of contaminated aquifer systems *(31)*.

The dispersion was sonicated for 5 minutes before injection. Prior to the test, the column was equilibrated by flushing with DI water, followed by water at the same background electrolyte concentration used later for particle injection. Then, the experiments included the injection of the colloidal dispersion at constant ionic strength, followed by flushing of the column in one or more steps for the release of deposited particles. Experiments were performed varying the ionic strength of the colloidal dispersion (DI water, 1 mM, 3 mM, 5 mM and 10 mM), the duration of the colloid injection (6 or 18 pore volumes, PVs), and the flow rate ($7.76 \cdot 10^{-5}$ m/s, $1.55 \cdot 10^{-4}$ m/s, $2.33 \cdot 10^{-4}$ m/s).

Two kinds of column tests were performed, including a short-lasting (6 PVs) and long-lasting (18 PVs) injection of ferrihydrite colloidal dispersion, named, respectively, “S” and “L” tests. More in

details, “S” tests included a first part at constant ionic strength, composed by (i) pre-conditioning of the column, (ii) injection of ferrihydrite particles (6 PVs), and (iii) flushing (6 PVs), followed by three further flushing steps, performed injecting (i) water at lower ionic strength (6 PVs), (ii) DI water (6 PVs), and (iii) high pH, obtained with NaOH 1mM (until breakthrough concentration reached zero). The test protocol is similar to the one applied for latex particles in Tosco et al. *(22)*. “L” tests were performed at constant ionic strength, including (i) pre-conditioning, (ii) injection of colloidal particles (18 PVs), and (iii) flushing. At the end of the test, the concentration of retained particles was determined. The column was extruded and dissected in 5 parts. For each part, the retained colloids were extracted by adding 17 ml of NaOH solution at 1mM, and sonicating for 5 minutes. Finally, the colloid concentration in the supernatant solution was determined via optical density measurements.

Measured data are reported in terms of a dimensionless normalized concentration s_{dep}:

$$s_{dep} = \frac{\rho_b}{n c_0} s \qquad (1)$$

where c_0 is the inlet colloid concentration [M L^{-3}], ρ_b is the bulk density of the porous medium [ML^{-3}], n is the (dimensionless) effective porosity [-], and s is the mass of deposited particles per unit mass of porous medium [M M^{-1}].

The tests are labelled basing on the different combinations of ionic strength applied to the colloidal dispersion (DI, 1mM, etc), injection duration (“S” and “L”), flow rate (1x, 2x and 3x for the three applied flow rates). The complete list of tests and the corresponding protocol is reported in the Supporting Information.

Estimation of attachment efficiency and travel distance

The Clean bed Filtration Theory (CFT) was developed for colloid transport under favourable deposition conditions, for the prediction of contact efficiency and therefore of attachment rates *(32)*. However, experimental evidence of deviation from the CFT was observed in the past. In particular, deviations were reported for the presence of unfavourable deposition conditions, when repulsive energy barriers can promote deposition in weak secondary minima, from which particles can then be released *(21-22, 33)*. Furthermore, the presence of discontinuities and impurities on the grain surface, which result in local variations of interaction potentials, can provide preferential deposition sites for colloidal particles, and give rise to spatial-dependent attachment rates *(18)*. Moreover, particle deposition at grain-to-grain contacts and in stagnation regions was shown to affect deposition kinetics *(33)*. All these factors require the introduction of correction coefficients and more complex models for the calculation of deposition rates *(21-22)*.

In this work, a simple relationship is desired for the estimation of particles travel distance under field conditions. For this reason, an average column attachment efficiency is introduced *(32)*

$$\alpha = -\frac{2}{3}\frac{d_{50}}{(1-n)\eta_0 L}\ln\left(\frac{c_{out}}{c_0}\right) \qquad (2)$$

where α is the attachment efficiency averaged over the whole column [-], η_0 is the single-collector contact efficiency *(34)* [-], d_{50} is the average sand diameter [L], and c_{out} is the breakthrough steady-state concentration [M L^{-3}] measured at a distance L from column inlet [L].

An empirical correlation that highlights the dependence of the attachment efficiency on ionic strength is *(35)*

$$\alpha = \frac{1}{1+\left(\frac{CDC}{I}\right)^{\beta}} \qquad (3)$$

where CDC is the critical deposition concentration [ML^{-3}], representing the ionic strength I [ML^{-3}] which separates unfavourable and favourable deposition regime, and β is an empirical

coefficient [-]. Both CDC and β can be determined via fitting of experimental attachment efficiencies, obtained from equation (2), reported vs ionic strength. Similar trends for deposition rates were also evidenced by the authors in a previous work *(22)*.

The distance that particles can travel in a porous medium under the same hydrological and hydrochemical conditions applied in column tests can be estimated from equation (2) as the distance within 99% of the particles are retained in the porous medium:

$$L_{0.01} = \ln(0.01)\frac{L}{\ln\left(\frac{c_{out}}{c_0}\right)} \quad (4)$$

Results and discussion

Electrokinetic properties of ferrihydrite particles and DLVO interaction energy profiles

The electrophoretic mobility of the ferrihydrite particles strongly depended on ionic strength. The measurements indicated a negative surface charge at neutral and basic pH, which can be attributed to the presence of residual adsorbed citrate, consistently with the literature *(36-37)*. Zeta potential values were obtained from the electrophoretic mobilities by applying the Smoluchowski equation *(38)*. Calculated values are -38.9±1.3 mV (DI water), -34.2±0.9 mV (NaCl 1 mM), -32.4±0.8 mV (NaCl 3 mM), -30.1±0.9 mV (NaCl 5 mM), -27.2±1.3 mV (NaCl 10 mM). For the high pH solution (NaOH 1mM) a zeta potential of -50.0±0.9 mV was obtained.

Zeta potentials for quartz sand were obtained from the literature, and were -40 mV (with DI water), -38.5 mV (at 1 mM NaCl), -30.8 mV (3 mM at NaCl), -28.3 mV (5 mM at NaCl), and -22.2 mV (10 mM at NaCl) *(39-40)*.

The data were used to calculate an estimate of particle-collector and particle-particle interaction profiles, following the DLVO theory *(32)*. For particle-collector interaction profiles (Figure 1), a repulsive energy barrier was found at all applied conditions. The repulsive peak is reduced at 5 mM

and 10 mM, suggesting that under these conditions some particles may overcome the barrier to deposit in the strong primary minimum. Conversely, at high pH the interaction profile is completely repulsive. Secondary negative minima, which are known to give rise to reversible deposition *(21-22)* were found for ionic strength in the range 1 to 10 mM, with absolute values lower than 1kT (being kT the product of the Boltzmann constant k and the temperature T, related to the average kinetic energy of the particles). Numerical values of minima and maxima are reported in the Supporting Information.

Influence of ionic strength on particle deposition and release

As a general rule, ferrihydrite particles were very mobile at low ionic strength, while increasing salt concentration decreased mobility, and consequently the amount of particles retained in the column increased (Figure 2 and Figure 3). During the deposition step, comparing tests performed at different ionic strengths showed that increasing ionic strength resulted in a retarded breakthrough curve and thus to an increased attachment rate. This is in agreement with common behaviour of negatively charged colloids *(21-22)*.

Detachment was negligible under constant ionic strength conditions ("L" tests and first step of "S" tests). A clear indication was the abrupt decline of all breakthrough curves at the end of particle injection (Figure 2 and Figure 3). This is also in agreement with steady state outlet concentrations, c_{out}/c_0, lower than 1 (Figure 4), which suggest that an equilibrium between deposition and release was not reached. Furthermore, the profiles of normalized concentration of deposited particles, s_{dep}, measured for "L" tests (Figure 3b), showed that particles were mainly retained within a short distance from the inlet, which is typical of irreversible deposition. The shape of the deposits cannot be explained by ripening phenomena in the late stages of deposition, because particle-particle

interaction potentials are repulsive (Supporting Information), and breakthrough curves did not show the typical decline in outlet concentration *(41-42)*. On the contrary, a possible explanation is a non uniform colloid population, characterized by minor variations in surface properties, and thus in interaction potentials, which may lead to differential deposition of the particles according to the travelled distance *(43)*.

The absence of relevant release phenomena is consistent with the limited depth of the secondary minima in the particle-collector interaction profiles *(21, 39)*, and consequently suggests that deposition should be mainly due to irreversible deposition mechanisms. However, the interaction profiles calculated for the ferrihydrite-silica system (Figure 1) exhibit a high repulsive barrier against deposition in the strong primary minimum. Irreversible straining is not likely to be a dominant deposition mechanism, due to the reduced particle size (the ratio of colloid to collector diameter is approximately equal to 0.001). On the contrary, surface roughness can enhance colloid entrapment at nano- and micro-scale cavities and asperities *(28, 44)*. Also small-scale heterogeneities on the surface of sand grains can play a role. Irregularities in the mineral structure as well as the presence of limited amount of other minerals (eg. K-feldspar) may lead to local charge variations, resulting in sites favourable to colloid deposition, or in interaction profiles with secondary minima deeper than those estimated for ferrihydrite-silica interaction *(33)*. Finally, it is worth to recall that the calculation of the interaction potentials relies on a number of approximations (see Supporting Information for details), thus providing an estimation of interaction trends, rather than quantitative values of potentials.

At the highest ionic strength (10 mM), the shape of the breakthrough curve during deposition is significantly different from other tests (Figure 2), and the concurrence of more than one deposition mechanism can be hypothesized. Deposition in the primary minimum is likely to occur for those particles characterized by higher kinetic energy, because the repulsive energy barrier in the ferrihydrite-silica interaction profile is close to the limit value of 15 kT *(45)* (Supporting

Information). This is in agreement with mass balances (Supporting information), which indicate that a fraction of particles was irreversibly retained.

Influence of flow rate on particle deposition and release

The flow rate did not significantly influence the colloid deposition at low ionic strength, when particle deposition rates were low. Conversely, when injecting particles at 5 mM (Figure 2b) and 10 mM (Figure 2c), the effects of flow rate were evident, both during deposition and release. As a general rule, particle deposition decreased with increasing flow rate, resulting in steeper breakthrough curves (Figure 2) and higher steady state concentrations (Figure 4). Release during flushing steps increased, which was consistent with previous research *(32, 46)*.

The deposited concentration profiles s_{dep} (Figure 3b) indicated that increasing flow rate strongly limited particle deposition, especially in the first part of the column (compare results for tests 10mM_L_2x and 10mM_L_3x). This can be associated to the mitigating effect on particle deposition of drag forces observed in the presence of repulsive energy barriers *(27, 41)*: particles weakly deposed in the secondary minimum were readily re-entrained by drag effects of the fluid. However, experimental results also indicate that the fraction of irreversibly retained colloids was not dramatically affected by flow rate (see mass balances), thus suggesting that irreversible deposition was not totally hindered at high flow rates.

Attachment efficiency and travel distance: dependence on ionic strength and flow rate

The attachment efficiency α and the corresponding travel distance $L_{0.01}$ were calculated from equations (2) and (4) respectively, for each column test where a steady state was reached during colloid deposition (Figure 5a and b). The experimental values of α (Figure 5a) show a clear dependence on both ionic strength and flow rate. The increase of α with increasing ionic strength is

well modelled by the empirical equation (2). Conversely, the influence of fluid velocity results in reduced α with increasing flow rate, which is consistent with previous literature *(33)*. The observed behaviour can be attributed to the micro-scale effects of hydrodynamic drag forces: under unfavourable deposition conditions, higher drag forces hinder particle deposition in the secondary minima, and conversely facilitate their release and re-suspension in bulk fluid. Experimental values of α were modelled with equation (2), determining the coefficients CDC and β via least square fitting. CDC was supposed independent on flow rate, because it is known to be influenced only by surface properties of porous medium and colloids *(32)*. As a consequence, the exponent β is the only parameter depending on fluid velocity. The inverse simulation provided β values of 1.26, 1.42, 1.65, respectively, for the three explored flow rates, which indicate a linear dependence of the exponent with flow rate. However, a data set covering a wider range of flow rates would be necessary to confirm the hypothesis. As for CDC, a value of 75.04 mM was obtained, which indicates that the ionic strength herein explored is far below the fast deposition region.

The travel distance $L_{0.01}$ showed an inverse correlation with the ionic strength, while increasing flow rate resulted in an increase in $L_{0.01}$, even if the influence was minor compared to the impact of ionic strength. In the typical range of clean groundwater ionic strength of approximately 2 to 5 mM *(29)*, the estimated $L_{0.01}$ was in the order of 10 to 20 m and decreased to few meters when ionic strength increased up to 10 mM (that is, for more contaminated aquifers).

A more general law can be derived for estimating the travel distance in the field under flow and hydrochemical conditions similar to those applied in column tests:

$$L_{0.01} = -\frac{2}{3}\frac{d_{50}}{(1-n)}\ln(0.01)\frac{1}{\eta_0(v)}\left[1+\left(\frac{CDC}{I}\right)^{\beta(v)}\right] \qquad (5)$$

In this equation, the dependence of $L_{0.01}$ on flow rate and ionic strength is highlighted. Ionic strength is explicitly included into the equation. Conversely, the flow rate influences the travel length through η_0 (details are provided in the Supporting Information) and the exponent β .

The travel distance calculated from (5) using the fitted values of CDC and β (solid lines in Figure 5b) evidenced the hyperbolic dependence of $L_{0.01}$ on ionic strength, and can be used for a first estimate of travel distance in field conditions.

Implications for field injection

The aim of ferrihydrite nanoparticles injection into contaminated aquifer systems is to create reactive zones or reactive barriers where the biodegradation of a wide range of contaminants is supported by a readily available Fe(III) source *(4, 9)*. Use of biopolymers or of other stabilizing agents is not required to prevent settling or aggregation of ferrihydrite nanoparticles, which is a great advantage for future field applications, in particular if compared to other iron-based nano- and microparticles used for contaminant degradation *(42, 47-48)*. In these cases, relevant pressures are required when delivering the products into the subsurface due to high fluid viscosity. Therefore, fracturing of the porous medium and the consequent formation of preferential flow paths are likely to occur. Conversely, the injection of ferrihydrite nanoparticles can be performed both by permeation or fracturing, and the distribution of the material in the aquifer medium can be controlled more easily.

Our data suggest that ferrihydrite mobility can be controlled by tuning the ionic strength of the suspension and the injection rate. If the ferrihydrite suspension is injected in the subsurface via permeation, for example using a direct-push technique, the flow rate distribution generating around the injection point is likely to ensure a reasonable radius of influence, at least of 3 to 6 meters, with

a quite uniform distribution of the material. Moreover, if the nanoparticles are desired not to travel far from the reactive zone, the colloidal suspension can be prepared adjusting the ionic strength to the value that provides the desired travel distance. In this sense, the proposed correlation for the estimation of travel distance can be a useful tool for rough estimations of the radius of influence of field injections. This might be of great benefit in the targeted forming of reactive zones of enhanced iron reduction, which can be set-up in the direction of groundwater flow and therefore contaminant migration. Also the ionic strength of the contaminated aquifer is to be carefully taken into consideration. Later, after the injection into the subsurface, ferrihydrite nanoparticles that deposited on the porous matrix are expected not to be washed out by the natural groundwater flow because column tests showed that particle release is not relevant unless in the presence of deionized water, or very high pH. In summary, our data open the perspective to directly target iron oxide nanoparticles to specific aquifer zones, where contaminant degradation can be precisely enhanced.

ACKNOWLEDGMENTS**:** The work was developed in the framework of the EU funded AQUAREHAB research project (FP7, Grant Agreement n. 226565). The authors thank prof. Daniele Marchisio at Politecnico di Torino for the permission to use the DLS instruments, and Miriam Ruggeri for the collaboration in column tests.

SUPPORTING INFORMATION AVAILABLE

Details on the experimental protocol and calculation of interaction profiles, numerical values of attachment efficiency, steady state concentration, travel distances and mass balances are provided in

the Supporting Information. This information is available free of charge via the Internet at http://pubs.acs.org/

Figures

Figure 1: Particle-collector interaction profiles for ferrihydrite colloids dispersed in DI water, water with adjusted ionic strength by addition of NaCl (1 mM, 3 mM, 5 mM, 10 mM), and high pH (NaOH 1mM). The windows shows the zooms of the primary (left) and secondary (right) energy minima.

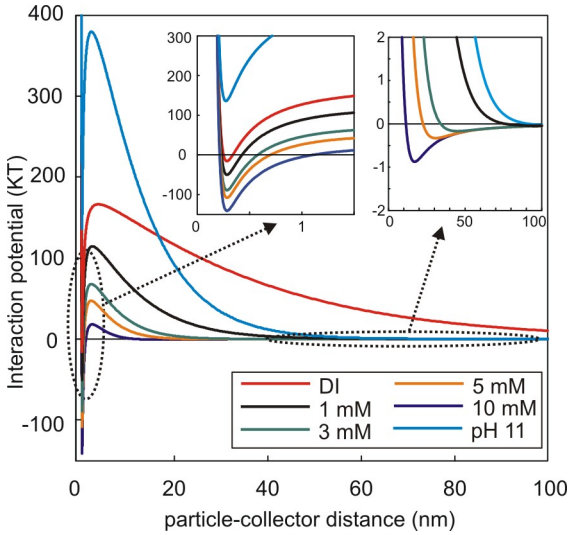

Figure 2: Breakthrough curves for short-lasting injection tests performed at the lowest flow rate (darcyan velocity equal to $7.76 \cdot 10^{-5}$ m/s), for all applied ionic strengths (a) and for ionic strength equal to 5 mM (b), and 10 mM (c) at all applied flow rates. The tests are labelled basing on the different combinations of ionic strength applied to the colloidal dispersion (DI, 1mM, etc), injection duration ("S" and "L"), flow rate (1x, 2x and 3x for the three applied flow rates).

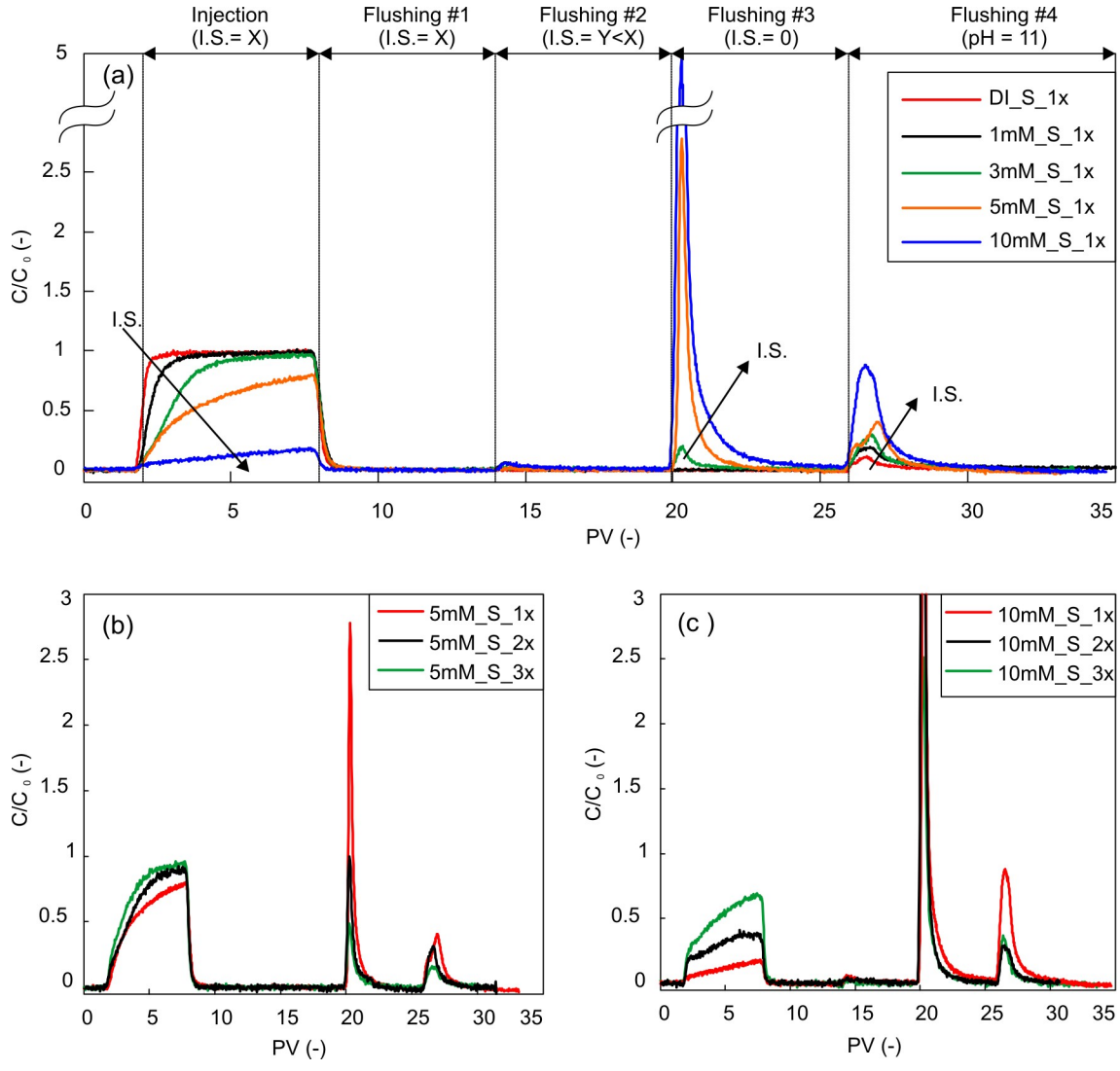

Figure 3: Breakthrough curves for long- lasting injection tests performed at 3 mM, 5 mM and 10 mM (a), at different flow conditions, and normalized concentration profiles of deposited particles along the columns at the end of the tests (b).

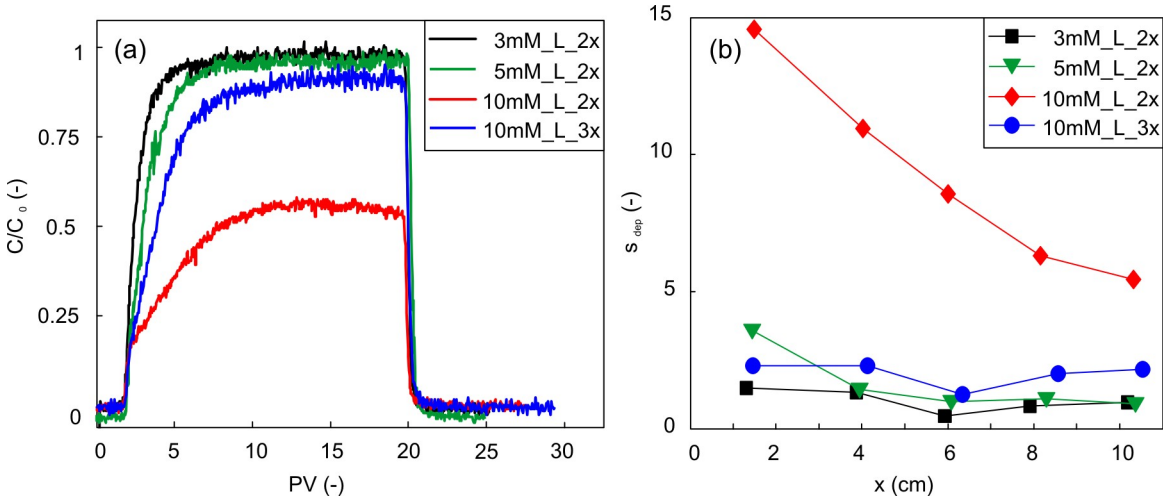

Figure 4: Steady state concentration c_{out}/c_0 versus ionic strength for both long- and short-lasting injection tests, for all those where the steady state concentration was reached before flushing.

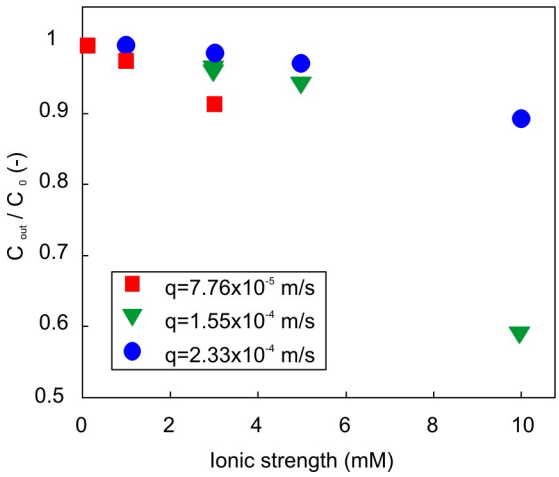

Figure 5: Average attachment efficiency (α) and travel distance ($L_{0.01}$) as a function of ionic strength and flow rate. Points are obtained, respectively, by applying eq (2) and (4) to experimental steady state concentrations. Lines correspond, respectively, to eq (3) fitted over experimental data and (5) calculated using fitted coefficients CDC and β.

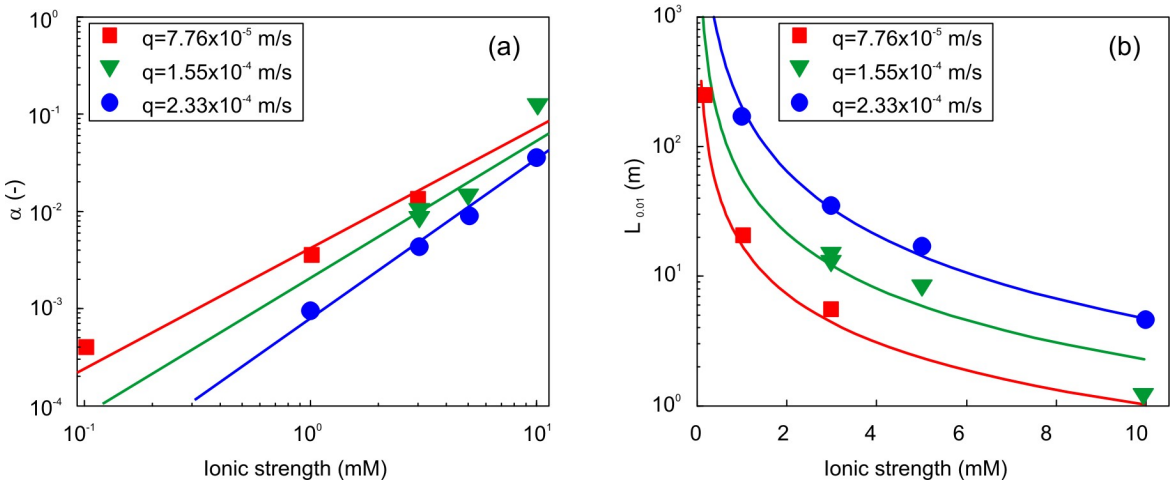

References

1. Banfield, J.F.; Zhang, H.Z. Nanoparticles in the environment. in *Nanoparticles and the Environment*; Mineralogical Soc America: Washington, 2001.
2. Hochella, M.F.; Lower, S.K.; Maurice, P.A.; Penn, R.L.; Sahai, N.; Sparks, D.L.; Twining, B.S. Nanominerals, mineral nanoparticles, and Earth systems. *Science* **2008**, *319*(5870), 1631-1635.
3. Gorski, C.A.; Nurmi, J.T.; Tratnyek, P.G.; Hofstetter, T.B.; Scherer, M.M. Redox behavior of magnetite: Implications for contaminant reduction. *Environmental Science and Technology* **2010**, *44*(1), 55-60.
4. Bosch, J.; Heister, K.; Hofmann, T.; Meckenstock, R.U. Nanosized Iron Oxide Colloids Strongly Enhance Microbial Iron Reduction. *Appl Environ Microb* **2010**, *76*(1), 184-189.
5. Bose, S.; Hochella Jr, M.F.; Gorby, Y.A.; Kennedy, D.W.; McCready, D.E.; Madden, A.S.; Lower, B.H. Bioreduction of hematite nanoparticles by the dissimilatory iron reducing bacterium *Shewanella oneidensis* MR-1. *Geochimica et Cosmochimica Acta* **2009**, *73*(4), 962-976.
6. Yan, B.; Wrenn, B.A.; Basak, S.; Biswas, P.; Giammar, D.E. Microbial reduction of Fe(III) in hematite nanoparticles by Geobacter sulfurreducens. *Environ. Sci. Technol.* **2008**, *42*(17), 6526-6531.
7. Weber, K.A.; Achenbach, L.A.; Coates, J.D. Microorganisms pumping iron: anaerobic microbial iron oxidation and reduction. *Nature Reviews Microbiology* **2006**, *4*(10), 752-764.
8. Waychunas, G.A.; Kim, C.S.; Banfield, J.F. Nanoparticulate iron oxide minerals in soils and sediments: unique properties and contaminant scavenging mechanisms. *J. Nanopart. Res.* **2005**, *7*(4-5), 409-433.
9. Bosch, J.; Fritzsche, A.; Totsche, K.U.; Meckenstock, R.U. Nanosized Ferrihydrite Colloids Facilitate Microbial Iron Reduction under Flow Conditions. *Geomicrobiol J* **2010**, *27*(2), 123-129.
10. Hansel, C.M.; Benner, S.G.; Nico, P.; Fendorf, S. Structural constraints of ferric (hydr)oxides on dissimilatory iron reduction and the fate of Fe(II). *Geochimica Et Cosmochimica Acta* **2004**, *68*(15), 3217-3229.
11. Tobler, N.B.; Hofstetter, T.B.; Straub, K.L.; Fontana, D.; Schwarzenbach, R.P. Iron-mediated microbial oxidation and abiotic reduction of organic contaminants under anoxic conditions. *Environmental Science & Technology* **2007**, *41*(22), 7765-7772.
12. Lovley, D.R. Microbial Fe(III) reduction in subsurface environments. *Fems Microbiology Reviews* **1997**, *20*(3-4), 305-313.
13. Lovley, D.R.; Anderson, R.T. Influence of dissimilatory metal reduction on fate of organic and metal contaminants in the subsurface. *Hydrogeology Journal* **2000**, *8*(1), 77-88.
14. Roling, W.F.M.; van Breukelen, B.M.; Braster, M.; Lin, B.; van Verseveld, H.W. Relationships between microbial community structure and hydrochemistry in a landfill leachate-polluted aquifer. *Applied and Environmental Microbiology* **2001**, *67*(10), 4619-4629.
15. Phenrat, T.; Saleh, N.; Sirk, K.; Tilton, R.D.; Lowry, G.V. Aggregation and sedimentation of aqueous nanoscale zerovalent iron dispersions. *Environmental Science & Technology* **2007**, *41*(1), 284-290.
16. Tiraferri, A.; Sethi, R. Enhanced transport of zerovalent iron nanoparticles in saturated porous media by guar gum. *J Nanopart Res* **2009**, *11*(3), 635-645.
17. Baalousha, M. Aggregation and disaggregation of iron oxide nanoparticles: Influence of particle concentration, pH and natural organic matter. *Science of the Total Environment* **2009**, *407*(6), 2093-2101.
18. Kretzschmar, R.; Borkovec, M.; Grolimund, D.; Elimelech, M. Mobile subsurface colloids and their role in contaminant transport. *Advances in Agronomy, Vol 66* **1999**, *66*, 121-193.
19. Johnson, P.R.; Sun, N.; Elimelech, M. Colloid transport in geochemically heterogeneous porous media: Modeling and measurements. *Environmental Science & Technology* **1996**, *30*(11), 3284-3293.

20. Bradford, S.A.; Yates, S.R.; Bettahar, M.; Simunek, J. Physical factors affecting the transport and fate of colloids in saturated porous media. *Water Resources Research* **2002**, *38*(12), Doi 10.1029/2002wr001340.
21. Tufenkji, N.; Elimelech, M. Breakdown of colloid filtration theory: Role of the secondary energy minimum and surface charge heterogeneities. *Langmuir* **2005**, *21*(3), 841-852.
22. Tosco, T.; Tiraferri, A.; Sethi, R. Ionic Strength Dependent Transport of Microparticles in Saturated Porous Media: Modeling Mobilization and Immobilization Phenomena under Transient Chemical Conditions. *Environmental Science & Technology* **2009**, *43*(12), 4425-4431.
23. Kuznar, Z.A.; Elimelech, M. Direct microscopic observation of particle deposition in porous media: Role of the secondary energy minimum. *Colloids and Surfaces a-Physicochemical and Engineering Aspects* **2007**, *294*(1-3), 156-162.
24. Chen, G.; Flury, M. Retention of mineral colloids in unsaturated porous media as related to their surface properties. *Colloids and Surfaces a-Physicochemical and Engineering Aspects* **2005**, *256*(2-3), 207-216.
25. Ko, C.-H.; Elimelech, M. The Shadow Effect in Colloid Transport and Deposition Dynamics in Granular Porous Media: Measurements and Mechanisms. *Environmental Science & Technology* **2000**, *34*(September 2000), 3681-3689.
26. Saleh, N.; Kim, H.J.; Phenrat, T.; Matyjaszewski, K.; Tilton, R.D.; Lowry, G.V. Ionic strength and composition affect the mobility of surface-modified Fe-0 nanoparticles in water-saturated sand columns. *Environmental Science & Technology* **2008**, *42*(9), 3349-3355.
27. Tong, M.; Johnson, W.P. Excess Colloid Retention in Porous Media as a Function of Colloid Size, Fluid Velocity, and Grain Angularity. *Environmental Science & Technology* **2006**, *40*(24), 7725-7731.
28. Johnson, W.P.; Pazmino, E.; Ma, H. Direct observations of colloid retention in granular media in the presence of energy barriers, and implications for inferred mechanisms from indirect observations. *Water Research* **2010**, *44*(4), 1158-1169.
29. Scheidleder, A.; Grath, J.; Winkler, G.; Stärk, U.; Koreimann, C.; Gmeiner, C.; Nixon, S.; Casillas, J.; Gravesen, P.; Leonard, J., et al., Groundwater quality and quantity in Europe. **1999**, European Environment Agency: Copenhagen.
30. Leibl, H.; Tomasits, R.; Bruhl, P.; Kerschbaum, S.; Eibl, M.M.; Mannhalter, J.W. Humoral and cellular immunity induced by antigens adjuvanted with colloidal iron hydroxide. *Vaccine* **1999**, *17*(9-10), 1017-1023.
31. Anneser, B.; Einsiedl, F.; Meckenstock, R.U.; Richters, L.; Wisotzky, F.; Griebler, C. High-resolution monitoring of biogeochemical gradients in a tar oil-contaminated aquifer. *Appl. Geochem.* **2008**, *23*(6), 1715-1730.
32. Elimelech, M. *Particle deposition and aggregation : measurement, modelling, and simulation*; Colloid and surface engineering series; Butterworth-Heinemann: Oxford [England] ; Boston, 1995.
33. Johnson, W.P.; Tong, M.; Li, X. On colloid retention in saturated porous media in the presence of energy barriers: The failure of α, and opportunities to predict η. *Water Resour. Res.* **2007**, *43*(12), W12S13.
34. Tufenkji, N.; Elimelech, M. Correlation equation for predicting single-collector efficiency in physicochemical filtration in saturated porous media. *Environmental Science & Technology* **2004**, *38*(2), 529-536.
35. Grolimund, D.; Elimelech, M.; Borkovec, M. Aggregation and deposition kinetics of mobile colloidal particles in natural porous media. *Colloid Surface A* **2001**, *191*(1-2), 179-188.
36. Fritzsche, A.; Bosch, J.; Rennert, T.; Heister, K.; Braunschweig, J.; Meckenstock, R.U.; Totsche, K.U. Fast microbial reduction of ferrihydrite colloids from a soil effluent. *Geochim Cosmochim Ac* **2012**, *77*(0), 444-456.
37. Hofmann, A.; Liang, L. Mobilization of colloidal ferrihydrite particles in porous media-An inner-sphere complexation approach. *Geochim Cosmochim Ac* **2007**, *71*(24), 5847-5861.
38. Hunter, R.J. *Foundations of colloid science*; 2nd ed; Oxford University Press: Oxford ; New York, 2001.

39. Redman, J.A.; Walker, S.L.; Elimelech, M. Bacterial Adhesion and Transport in Porous Media: Role of the Secondary Energy Minimum. *Environmental Science & Technology* **2004**, *38*(6), 1777-1785.
40. Kosmulski, M.; Maczka, E.; Janusz, W.; Rosenholm, J.B. Multiinstrument study of the electrophoretic mobility of quartz. *Journal of Colloid and Interface Science* **2002**, *250*(1), 99-103.
41. Li, X.; Zhang, P.; Lin, C.L.; Johnson, W.P. Role of Hydrodynamic Drag on Microsphere Deposition and Re-entrainment in Porous Media under Unfavorable Conditions. *Environmental Science & Technology* **2005**, *39*(11), 4012-4020.
42. Tosco, T.; Sethi, R. Transport of non-newtonian suspensions of highly concentrated micro- and nanoscale iron particles in porous media: A modeling approach. *Environmental Science and Technology* **2010**, *44*(23), 9062-9068.
43. Li, X.Q.; Scheibe, T.D.; Johnson, W.P. Apparent decreases in colloid deposition rate coefficients with distance of transport under unfavorable deposition conditions: A general phenomenon. *Environmental Science & Technology* **2004**, *38*(21), 5616-5625.
44. Auset, M.; Keller, A.A. Pore-scale visualization of colloid straining and filtration in saturated porous media using micromodels. *Water Resources Research* **2006**, *42*(12).
45. Prieve, D.C.; Lin, M.M.J. Adsorption of brownian hydrosols onto a rotating disc aided by a uniform applied force. *Journal of Colloid and Interface Science* **1980**, *76*(1), 32-47.
46. Tufenkji, N.; Miller, G.F.; Ryan, J.N.; Harvey, R.W.; Elimelech, M. Transport of Cryptosporidium oocysts in porous media: Role of straining and physicochemical filtration. *Environmental Science & Technology* **2004**, *38*(22), 5932-5938.
47. Dalla Vecchia, E.; Luna, M.; Sethi, R. Transport in Porous Media of Highly Concentrated Iron Micro- and Nanoparticles in the Presence of Xanthan Gum. *Environmental Science & Technology* **2009**, *43*(23), 8942-8947.
48. Borum, E., Bioremediation of Chlorinated Solvents in Fractured Bedrock: Characterization and Case Studies. **2002**, U.S. Environmental Protection Agency, Office of Solid Waste and Emergency Response: Arlington, VA.